Journal of Applied Physics ARTICLE scitation.org/journal/jap

An effective method of reconnoitering current–voltage (*IV*) characteristics of organic solar cells

Cite as: J. Appl. Phys. **132**, 015001 (2022); doi: 10.1063/5.0089706
Submitted: 28 February 2022 · Accepted: 8 June 2022 ·
Published Online: 5 July 2022

Rico Meitzner,[1,2,a)] Jose Prince Madalaimuthu,[1,2] Shahidul Alam,[1,2,3] Md Moidul Islam,[1,2] Sebastian Peiler,[1,2] Aman Anand,[1,2] Johannes Ahner,[2] Martin D. Hager,[1,2] Ulrich S. Schubert,[1,2] Yingping Zou,[4] Frédéric Laquai,[3] and Harald Hoppe[1,2]

AFFILIATIONS

[1]Center for Energy and Environmental Chemistry Jena (CEEC Jena), Friedrich Schiller University Jena, 07743 Jena, Germany
[2]Laboratory of Organic and Macromolecular Chemistry (IOMC), Friedrich Schiller University Jena, 07743 Jena, Germany
[3]King Abdullah University of Science and Technology (KAUST), KAUST Solar Center (KSC), Physical Sciences and Engineering Division (PSE), Thuwal 23955-6900, Kingdom of Saudi Arabia
[4]College of Chemistry and Chemical Engineering, Central South University, Changsha 410083, China

[a)]**Author to whom correspondence should be addressed:** rico.meitzner@uni-jena.de

ABSTRACT

Current–voltage (*IV*) characterization is the most fundamental measurement performed on solar cells. This measurement is commonly used to extract basic solar cell parameters, such as open circuit voltage, short circuit current density, fill factor, and power conversion efficiency. We were able to obtain a fast tool to find defective behavior using Simulation Program with Integrated Circuit Emphasis simulations and generate an understanding of which device property can create such defective behaviors by analyzing the second derivative of *IV* curves.

I. INTRODUCTION

Organic solar cells represent a highly promising technology for the future of sustainable energy.[1–3] Due to their specific applicability for agrivoltaic applications, they can enable rapid electrification, particularly in more remote locations.[4–6] Recently, they have achieved 18% Power Conversion Efficiency (PCE) on lab scale[7] and around 14% on module scale.[3] They can obtain a very low environmental footprint[8,9] and have shown that they are able to achieve long lifetimes sufficient for market entry.[10,11] Their development is, for the moment, still driven mainly by serendipity, as many metrics of their materials cannot easily be predicted just from their structure. Hence, many compounds have to be synthesized and the properties have to be experimentally determined.

The most basic measurement with which every solar cell is evaluated is a current–voltage (*IV*) characterization, where the solar cell is measured under an AM1.5G compatible light source, to determine its performance. The solar cell under these circumstances should behave like a diode under illumination and should, therefore, follow the Shockley equation[12] with an additional term for the series and shunt resistance that a real solar cell always has,

$$I = I_L - I_0\left\{\exp\left(\frac{q(V+IR_S)}{nk_BT}\right) - 1\right\} - \frac{V+IR_S}{R_{Sh}}, \quad (1)$$

with I being the current, I_L the photocurrent, I_0 the dark saturation current, q the elementary charge, V the applied voltage, R_S the series resistance, n the diode ideality factor, k_B the Boltzmann constant, T the temperature, and R_{Sh} the shunt resistance.

Any deviation from the behavior of an ideal diode is usually associated with performance losses. Hence, the shape of the *IV* curve is also the most fundamental indicator of a well-functioning or aberrant device. Obtaining a better understanding of aberrations in an *IV* curve can be the first step to understand which part of the device/layer stack is not working as expected. A usual way to do so can be simulations of the *IV* behavior. A well-established tool to do so is SPICE[13–15] (Simulation Program with Integrated Circuit Emphasis), which allows to model equivalent circuits of solar cells.

It has already been widely used in the analysis of organic solar cells. For example, Zuo *et al.* used an equivalent circuit model to understand the occurrence of S-shapes in vacuum processed organic solar cells in dependence on the anode buffer layer that

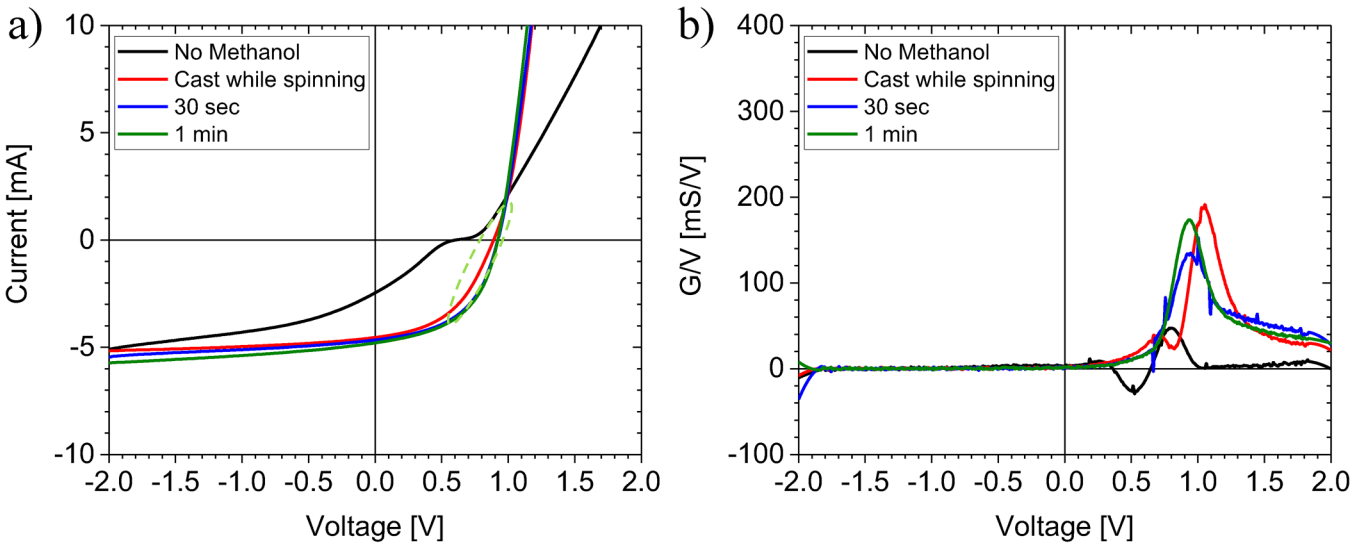

FIG. 1. *IV* curves (a) of PCDTBT:$PC_{71}BM$ based organic solar cells without and with an overcast of methanol done on top of the active layer and their respective second derivatives (b).

was used.[16] They, thereby, found that their results were best explained by assuming a Schottky contact at the interface to the anode buffer layer and the active layer. Yoo *et al.* studied light dependence of organic solar cell performance via the usage of equivalent circuit models.[17] They found that it was not possible to sufficiently describe their experimental results with a circuit model containing only a single diode and a single shunt resistance, but instead, they had to add a second one of each of these components, showing light-dependent parameters. Though they also stated that from these fitting parameters alone, it is not sufficiently possible to draw conclusions about individual physical processes occurring in the solar cell and more sophisticated methods have to be applied to gain a deeper understanding of the processes.

Qi *et al.* studied the changes in fill factor (FF) in organic solar cells using equivalent circuit models. They modeled the impact of series and shunt resistances, as well as of dark saturation current density and diode ideality factor on the FF. Furthermore, they studied how the S-shapes can be explained with equivalent circuit models and concluded that the various physical processes that can result in an S-shape in the end still result in a common effect, which is a reduction in the internal electric field due to charge accumulation and, thereby, hinder charge carrier extraction and increase recombination. Ecker *et al.* also studied the impact of light soaking on inverted organic solar cells with a titanium oxide electron transport layer (ETL) via the usage of equivalent circuit models.[18] They proposed a circuit with multiple capacitances, where one was associated with the TiO_x layer, while another one with the capacitance of the active layer. They found that upon light soaking, the capacitance of the active layer is reduced due to a reduction of resistance of the TiO_x layer, therefore increasing the internal electric field in the active layer and helping with charge extraction.

S-shapes in the *IV* curves of organic solar cells are a well-known deviation from ideality.[12,13,19] They can be caused by blocking contacts, reductions of charge carrier mobility of one charge carrier, space charge zones, for example, due to the accumulation of trapped charge carriers, and limited surface recombination at any of the charge extraction layers. Besides the S-shapes, there can also be more subtle abnormalities,[20,21] which nonetheless reduce the overall

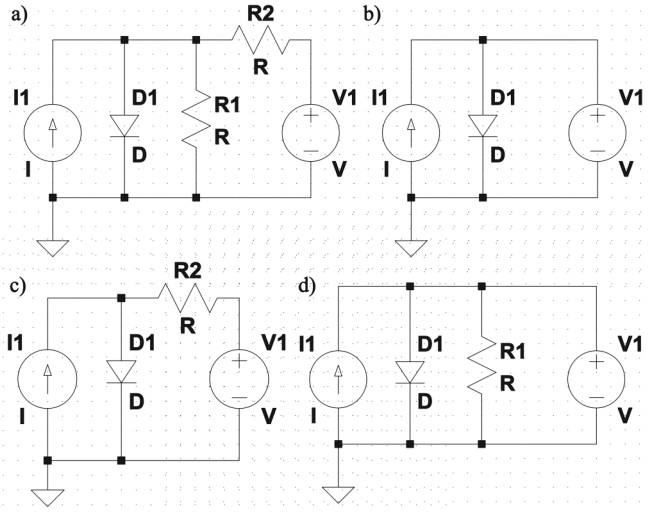

FIG. 2. Equivalent circuits of solar cells in LTSpice: (a) Standard equivalent circuit of a solar cell with photocurrent (I1), Diode (D1), Shunt Resistance (R1), Series Resistance (R2); (b) circuit used to evaluate the impact of dark saturation current and diode ideality factor on the second derivative of the *IV* curve; (c) circuit used to evaluate the impact of series resistance on the second derivative; (d) circuit used to evaluate the impact of shunt resistance on the second derivative.

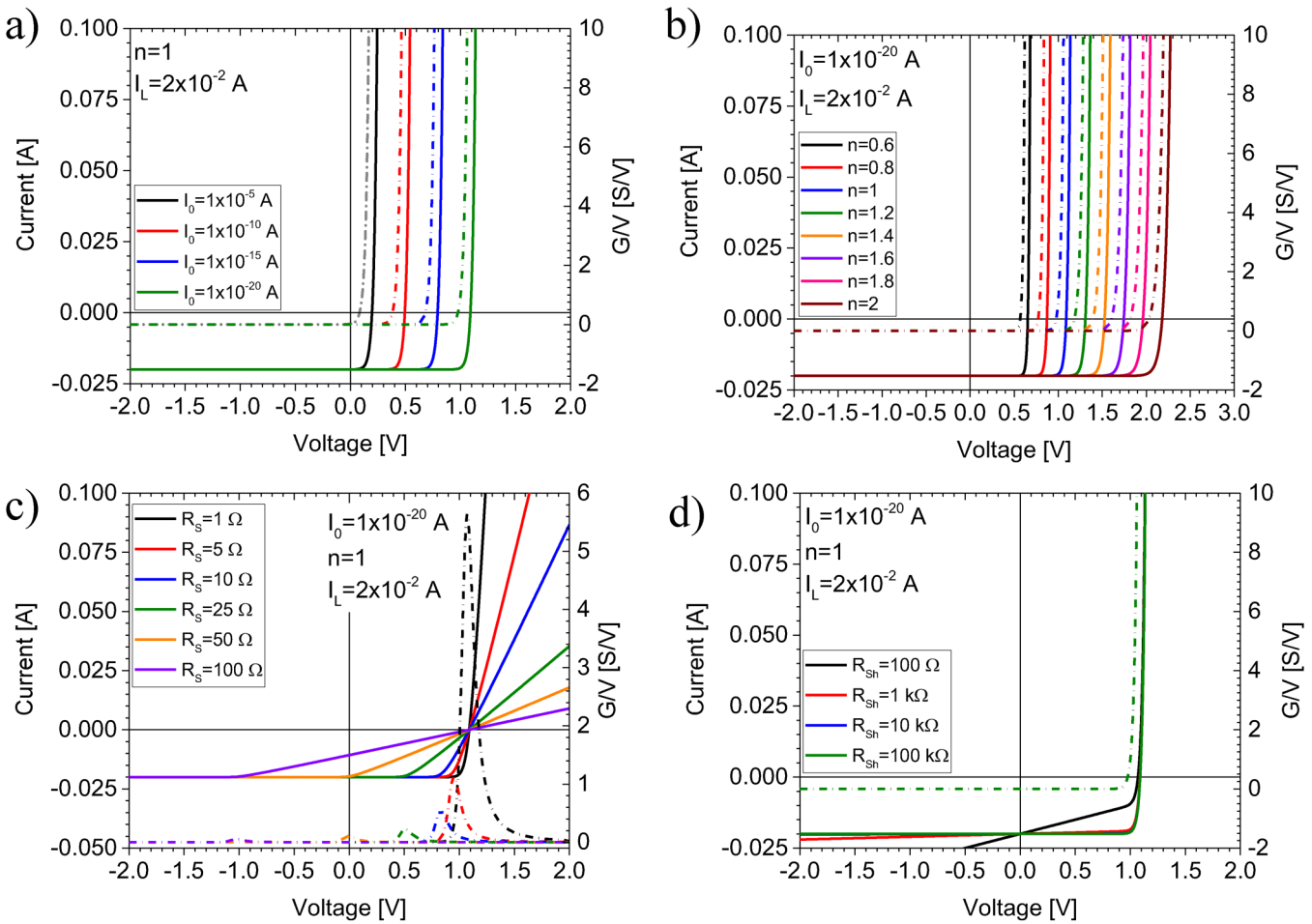

FIG. 3. *IV* curves simulated in LTSpice plus their respective second derivatives: (a) impact of dark saturation current variation; (b) impact of diode ideality factor variation; (c) impact of series resistance variation; (d) impact of shunt resistance variation.

performance of a device, and actually for an aged device, might be an early indicator of further degradation in the future.

The scope of this paper is to present an additional and new way on how to analyze data obtained from *IV* characterizations. On the one hand, we determined the second order derivatives of the *IV* curves in order to emphasize the characteristics of the measured curves. On the other hand, however, we used SPICE,[15] in order to address electric circuits and their *IV* characteristics. This enables us to narrow down the type of particular appearing defects. Thus, we are able to apply only the really required sophisticated methods to study device defects in organic solar cells and analyze them faster.

II. EXPERIMENTAL

A. Materials

ITO glass was obtained from Xinyan Technology Ltd. and had a sheet resistance of 10 Ω/sq. The PEDOT:PSS [poly(3,4-ethylenedioxythiophene) polystyrene sulfonate] used was Clevios PH from Heraeus for unaged devices; for the devices on which aging was performed, PVP AI 4083 was used. As donor polymer PCDTBT (poly[9-(1-octylnonyl)-9H-carbazole-2,7-diyl]-2,5-thiophenediyl-2,1,3-benzothiadiazole-4,7-diyl-2,5-thiophenediyl], poly[N-9′-heptadecanyl-2,7-carbazole-alt-5,5-(4′,7′-di-2-thienyl-2′,1′,3′-benzothiadiazole)]) obtained from 1-material was used. The acceptor used was $PC_{71}BM$ ([6,6]-phenyl-C71-butyric acid methyl ester) that was obtained from nano-C. A solution of PCDTBT:$PC_{71}BM$ in CF:CB (1:1) was prepared two weeks before the processing of the devices. The PCDTBT concentration was 5 mg/ml and the ratio between PCDTBT and $PC_{71}BM$ was 1:2; it was kept at 50 °C and stirred at 700 rpm. For the devices shown in Figs. 10 and S2 in the supplementary material, solutions of TTFQx-T1:$PC_{71}BM$, TTFQx-T1:ITIC, HFAQx-T:$PC_{71}BM$, and HFAQx-T:ITIC were prepared in the glovebox with a ratio of 1:1.5 in chlorobenzene. The solutions were kept stirred overnight on a hot plate at 50 °C.

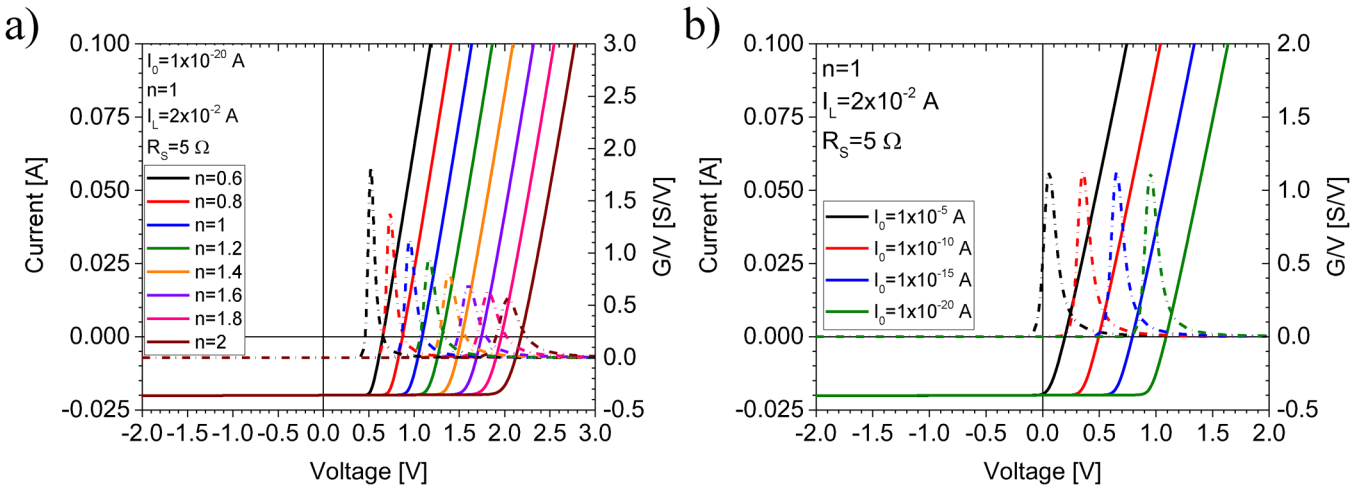

FIG. 4. Combined impact of series resistance and (a) diode ideality factor and (b) dark saturation current.

B. Processing

Substrates were cleaned by first sonification of the ITO glass substrates in toluene for 15 min, followed by sonification for another 15 min in isopropanol. Following this, the substrates were dried with dry nitrogen. PEDOT:PSS was coated via spin coating on the substrates at 3000 rpm for 35 s. Each sample was structured via the usage of a moist cotton tip and annealed at 178 °C for 15 min. After annealing, they were immediately transferred into a nitrogen glovebox. PCDTBT:$PC_{71}BM$ solution was spin-cast on the PEDOT:PSS at 1200 rpm for 45 s. For different sample processing, methanol was either applied after active layer processing or not. For the samples with methanol treatment, they were either spun up again and methanol was dropped onto the spinning active layer or the samples were at rest. Methanol was dropped on the active layer and the sample was spun again for either 30 s or 1 min. After methanol was initially dropped onto the sample, for aged devices, the active layer was post-treated with methanol for 45 s. After the active layer processing and potential post-treatment, the samples were transferred to a shadow mask and placed into a vacuum chamber to thermally evaporate an aluminum electrode. At a pressure below 5E-5 mbar, a 200 nm thick Al electrode was deposited onto the samples. Following, the samples were sealed with a glass slide and UV curable epoxy glue.

Processing for the devices in Figs. 10 and S2 in the supplementary material followed a similar procedure as with the PCDTBT:$PC_{71}BM$ devices, with the following alterations; for TTFQx-T1:$PC_{71}BM$ solutions, before spin casting, 0.5 vol. % DIO was added; TTFQx-T1:ITIC devices were thermally annealed at 150 °C for 10 min inside the glovebox; for HFAQx-T:$PC_{71}BM$ solutions, before spin casting, 0.25 vol. % DIO was added; HFAQx-T:ITIC devices were thermally annealed at 130 °C for 10 min inside the glovebox. Additionally, in these devices, a Mg layer of 50 nm thickness was thermally evaporated before the deposition of the Al electrode.

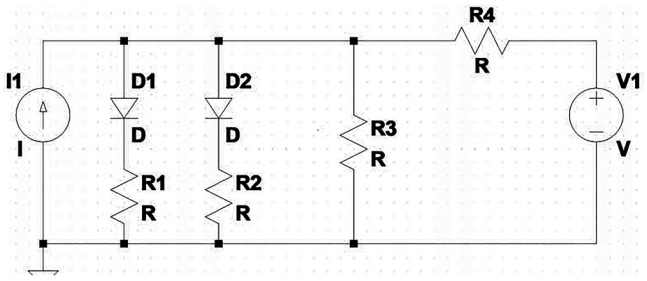

FIG. 5. Equivalent circuit in LTSpice to study the origin of abnormal behavior of the *IV* curve in the devices seen in Fig. 1.

C. Characterization

Samples were characterized using a solar simulator (Wavelabs Sinus 70) calibrated at an intensity of 1 sun and with an AM 1.5G spectrum. A SMU (Keithley 2400) was used to record the *IV* curves, the settings were NPLC of 1, a wait time of 10 ms, and a measurement range of −2 to 2 V split into 10 mV measurement intervals. Samples were aged in a custom setup at 45 °C ambient temperature and under a white light LED, compatible with ISOS-L1 protocols.[23,24] Aged samples were measured and automated at 30 min intervals with a sweep range from −2 to 2 V in 10 mV intervals, with an NPLC of 1 and a wait time of 10 ms. A Keithley 2700 SMU was used in combination with a multiplexer from Keithley.

Anfatec Instruments AG (Germany) single-point Kelvin Probe (KP) system was used for work function measurements. All of the measurements were carried out in the open air. The KP system was calibrated using highly oriented pyrolytic graphite (HOPG) with a known work function of 4.46 (±) 0.04 eV. HOPG was freshly sliced

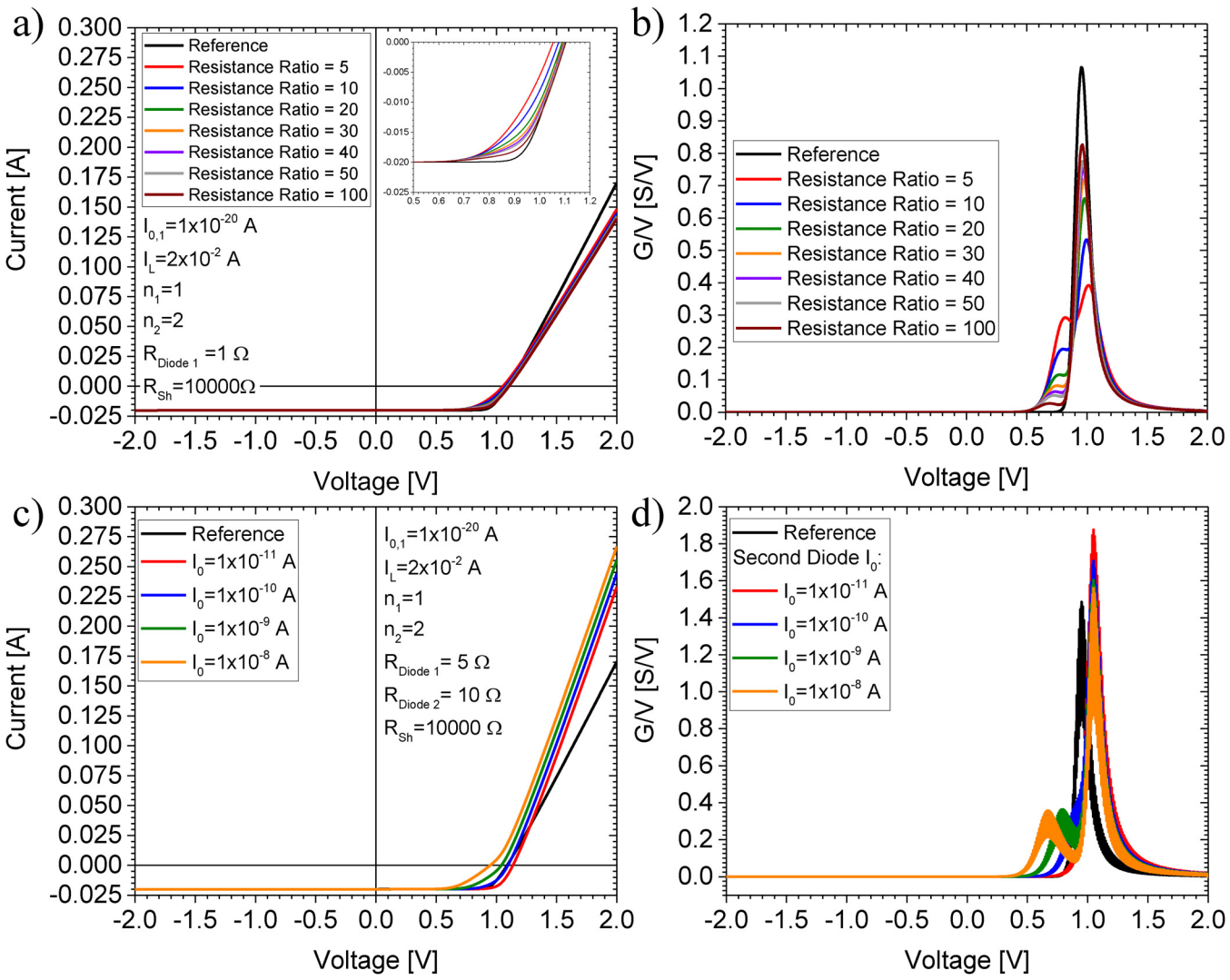

FIG. 6. Simulation results from LTSpice for the equivalent circuit shown in Fig. 5. There are clearly two distinct peaks visible, whose position and ratio can be neatly modified by the proper choice of parameters; (a) *IV* curves for the variation of resistance ratio between R1 and R2, the inset is showing a close up of the *IV* curves around the maximum power point; (b) respective second derivative of the *IV* curves in (a); (c) *IV* curves for the variation of dark saturation current of the weak performing diode.

with the use of a sticky tape for each calibration of the KP system, exposing a pristine graphite surface.

D. Simulations

All equivalent circuits in this paper were simulated using the software LTSpice,[25] due to its free-of-cost availability and compatibility with various operating systems.

III. RESULTS AND DISCUSSION

In Fig. 1, the *IV* curves of conventional organic solar cells based on an active layer of PCDTBT:$PC_{71}BM$ are shown. The cells were treated with methanol after spin casting the active layer. On the basis of an earlier work, we knew that treatment with methanol is able to reduce the S-shape character of the *IV* curve of an organic solar cell.[22] The first *IV* curve in Fig. 1(a) shows a cell where no methanol was used as a post active layer processing step and one can see a clear S-shape in the *IV* curves of all the cells on this device. In Fig. 1(a), the second *IV* curve shows the cell where after the active layer deposition, 1 ml of methanol was dropped on the active layer while the substrate was spinning. One can clearly see an improvement in the device characteristics, but there is still only a weakly visible kink around the maximum power point (MPP) of the cells, which is marked with a light green oval. To get

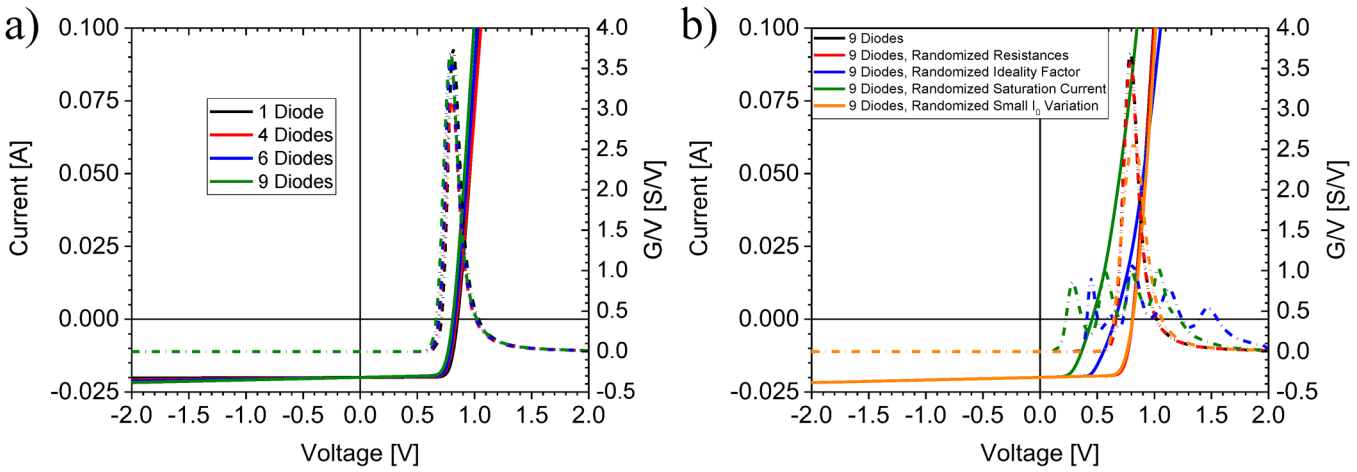

FIG. 7. *IV* curve simulations of circuits containing multiple sub-solar cells as shown in Fig. 2(a). For more details, see the supplementary material; (a) identical parameters for all sub-solar cells, overall device series resistance kept constant and (b) increased variation of sub-solar cell variation.

a better picture—if this kink might still be a very weak S-shape—we calculated the second derivative of the *IV* curve, as an S-shape should have an inflection point and should, therefore, show up as a crossing of the voltage axis in the second derivative. The second derivative for this cell is shown in (b), and it can be seen that there is no crossing of the voltage axis; instead, there is only a flat spot. From the second derivative of the first *IV* curve seen in Fig. 1(a), which is shown in (b), one can clearly see that an S-shape is also resulting in a crossing of the voltage axis. For the last two cells shown in Fig. 1(a), methanol was dropped on the active layer after its processing and the devices were kept coated with methanol for either 30 s or up to 1 min before it was spun off the films. For both of these devices, the flat spot in the *IV* curve visible as a valley in the second derivative disappeared, and only a single peak remained, which was above the value of the open-circuit voltage of the devices.

To gain a better understanding of what these different shapes of second derivatives mean for the processes happening in the solar cell, we performed simulations of the *IV* curves via the usage of SPICE. First, we wanted to understand the contributions of different circuit elements in the standard equivalent circuit used for solar cells on the second derivative. Figure 2 shows the different equivalent circuits we used in SPICE, (a) is the well-established equivalent circuit of a solar cell with a photocurrent source (I1), a diode (D1), a shunt resistance (R1), and a series resistance (R2); (b) was the circuit used to gain an understanding of the parameters impacting the second derivative in terms of the diode parameters, with only a diode being present. Furthermore, (c) and (d) were the basis for studying the impact of either series or shunt resistance on the second derivative.

In Fig. 3, the simulated *IV* curves and their respective second derivatives are shown, (a) and (b) are based on simulation results done with the circuits shown in Fig. 2(b), while for Fig. 3(a), the diode ideality factor n was kept constant and the dark saturation current I_0 was varied for (b) I_0 was kept constant, while n was varied. The variation of I_0 and n only results in a shift of where the second derivative is starting to increase, which is an expected result, as without series and shunt resistance, the diode equation is a simple exponential function and will keep its principle shape even after derivation only with a modified pre-factor. Figure 3(c) shows the simulation results for the circuit shown in Fig. 2(c) with R_S added; here, I_0 and n were kept constant, while R_S was varied. The second derivative in this case shows a clear peak around the open-circuit voltage of the simulated *IV* curve and it is qualitatively similar to the second derivative of the solar cells *IV* curves shown in Figs. 1(f) and 1(h). This peak can be understood when looking at what the second derivative represents, namely, a change in conductivity with the applied bias. The only element in the circuit showing a bias-dependent conductivity is the diode. Because for increasing voltage bias, the diode behavior dominates the *IV* characteristic, and thus, the increasing bias causes an increase in current density. For a greater voltage bias, however, the ohmic part of the series resistant will start to govern the *IV* characteristic. Because of the linear relation between current and voltage for an ohmic resistor, the second derivative of the current with respect to voltage bias is zero, which is why the whole *IV* characteristic of the solar cells becomes zero for sufficient great bias; thus, the increasing current for diode-governed bias and decreasing current until zero for ohmic-governed bias explain why in any real solar cell the second derivative of the *IV* curve is expected to show a peak. This

TABLE I. Possible impacts of methanol washing on the active layer.

Hypothesis	"Short-term"	"Long-term"	Probability
Removal of impurities	x	X	Possible
Formation of a SAM	x	X	Low
Stratification of active layer		X	Possible

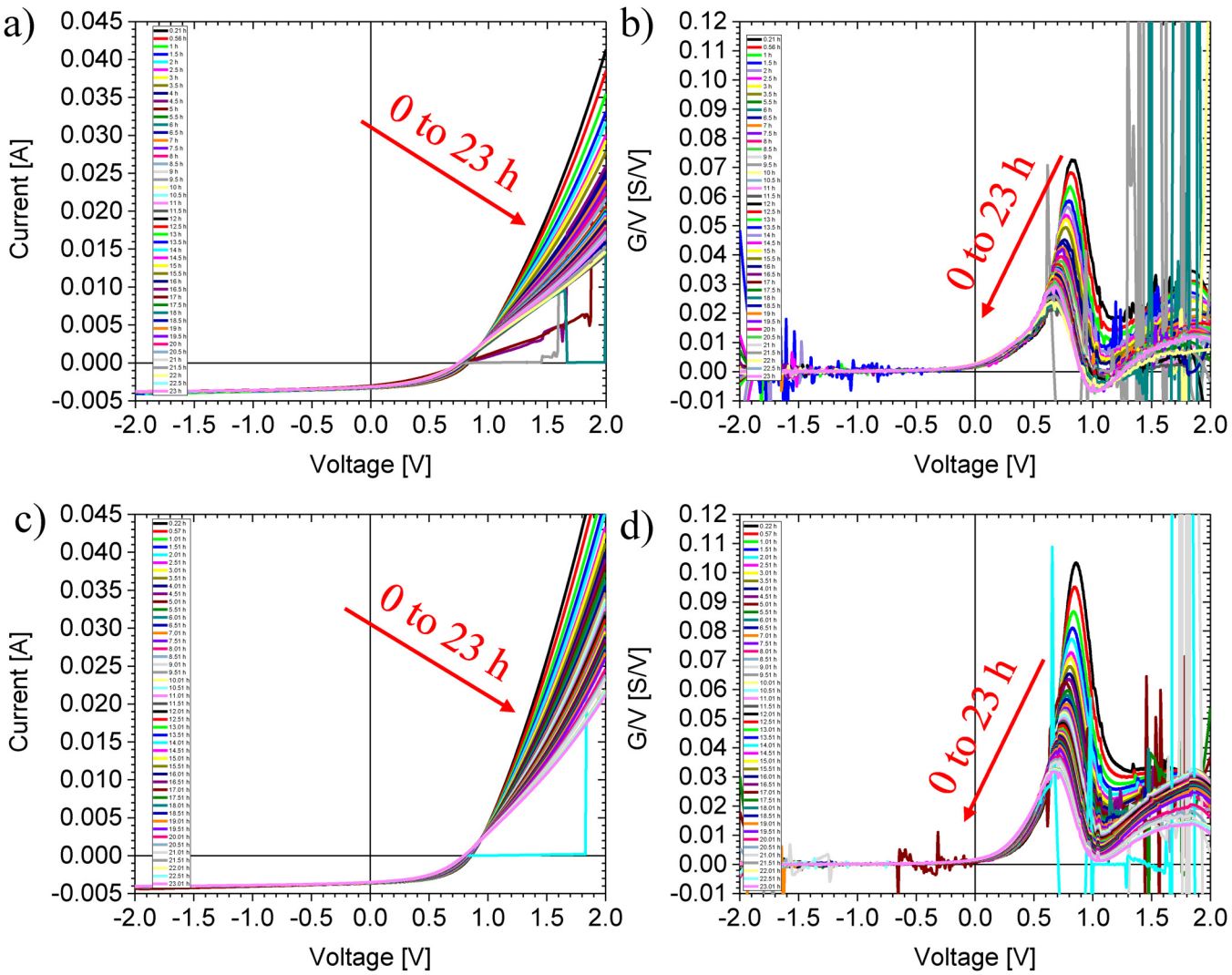

FIG. 8. *IV* curves and their respective second derivatives for organic solar cells (OSCs) of the first 24 h, aged under ISOS-L1 conditions. Each curve was measured automatically every 30 min. For the second derivative, some curves were plotted with 90% transparency for better visibility. (a) *IV* curve for the device developing a blocking contact within 24 h; (b) respective second derivative; (c) device is not developing a blocking contact within 24 h; (d) respective second derivative.

behavior can be witnessed for the second order derivatives. Figure 3(d) shows the *IV* curve of the simulation done with the equivalent circuit shown in Fig. 2(d). All the curves shown for the second derivative are on top of each other, i.e., they do not vary with shunt resistance, as all the other parameters were constant for these simulations. This result can be easily understood as the term for shunt resistance in the diode equation is a linear term, i.e., it disappears after twice differentiating the equation.

From Fig. 3(c), we saw some interesting interactions between the diode in the circuit and the series resistance on the second derivative of the *IV* curve, i.e., a peak started to form. For a better understanding of the shape and position of this peak, we further studied the interplay between series resistance, dark saturation current, and diode ideality factor. The results of these simulations can be seen in Fig. 4; the equivalent circuit used was the same as for Fig. 3(c). In Fig. 4(a), the impact of the diode ideality factor can be seen on the height, position, and width of the peak in the second derivative—an increase in n results in a reduction in peak size, a shift in peak position toward higher voltages, and an increase in the overall width of the peak. Figure 4(b), on the other hand, shows the impact of dark saturation current on the peak, and the only impact this parameter has is a shift in peak position with a shift toward higher voltages with a reduction in dark saturation current.

From previous simulations, we saw that a combination of the series resistor and diode results in a peak in the second derivative.

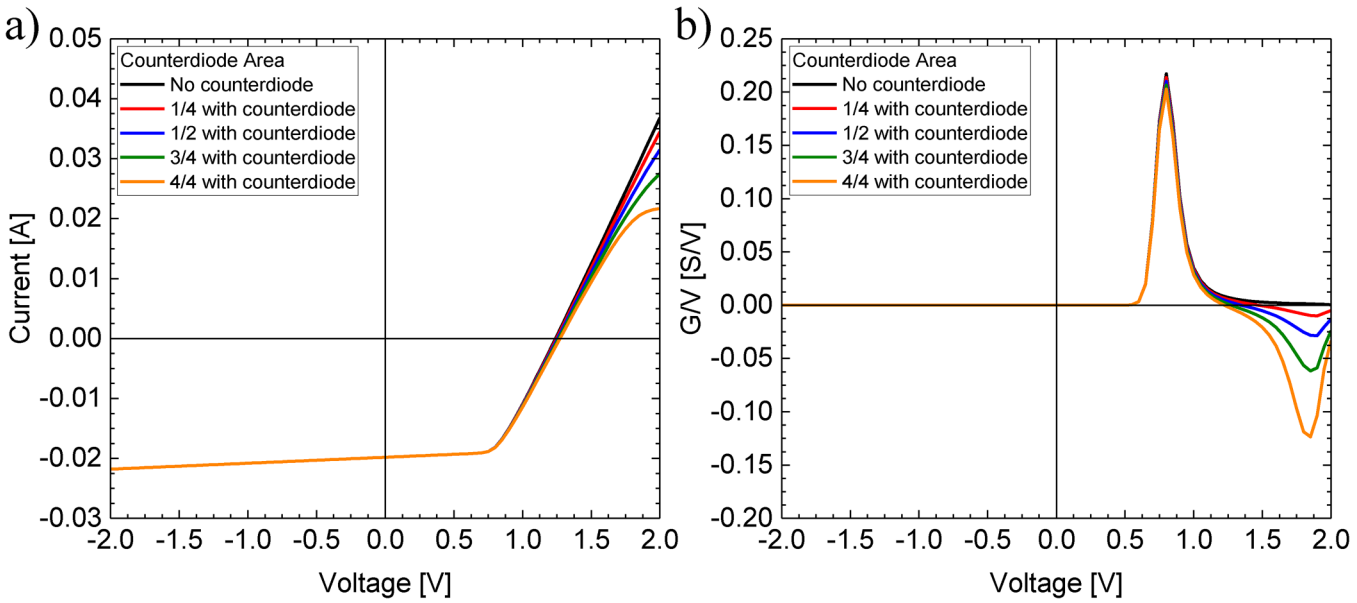

FIG. 9. Simulation of the formation of a blocking contact over time. (a) *IV* curves from SPICE simulation, (b) Respective second derivatives of the *IV* curves from (a).

This showed that for the shape of the second derivative found for the solar cell with a simple overcast of methanol while spinning, shown in Fig. 1(b), it is required to have two diodes in parallel, to see such a feature of the main peak with an associated side peak. For evaluation of such a phenomenon, we simulated the circuit seen in Fig. 5 in LTSpice.

The resulting *IV* curves of the aforementioned simulations are shown in Fig. 6. As we already saw from Figs. 3(c) and 4, there is a combined impact on the shape of the peak in the second derivative of the *IV* curves from the interaction of I_0, n, and R_S, and we performed multiple simulations where we modified these parameters between two diodes. Thereby, we assumed the diodes to perform worse than the other; hence, we inherently set the dark saturation current of the second diode significantly lower than that of the well-functioning diode. The results of these simulations can be seen in Fig. 6. In (a) and (b), we varied the ratio of resistance associated with the respective diodes. We assumed that the regions with a well-functioning diode should generally show a low contact resistance and should, therefore, have an inherently lower resistance than the badly functioning diode, which shows a high dark saturation current and, therefore, much leakages. From (a), one can see that the parallel diode with a large dark saturation current results in a reduction in the fill factor. This reduced fill factor is more pronounced when the associated contact resistance of the diode is better, i.e., lower, as this results in a larger current flow across the defective diode. From the associated second derivative shown in Fig. 6(b), one can see that the second diode indeed results in a secondary peak, which shifts toward lower voltages with an increased contact resistance and additionally reduces in peak height, while the main peak increases with a reduction in the secondary peak height. In Figs. 6(c) and 6(d), the resistance ratio between the two diodes is kept constant, but the dark saturation current of the secondary diode was increased. Again, this increase results in a clear reduction of the fill factor and also the open-circuit voltage, once the secondary diode's dark saturation current has increased sufficiently enough. With regard to the second derivative, see Fig. 6(d), a secondary peak can be seen and with an increase in the dark saturation current of the defective diode, that secondary peak shifts toward lower voltages, while the main peak is reduced in height.

The simulation results in Fig. 6 can successfully reproduce the shape of the second derivative seen for the device shown in Fig. 1 with only methanol overcast during spinning, though they are quantitively not sufficient. In principle, as a real device consists of many diodes in parallel to each other, we created several increased equivalent circuit models based on multiple parallel-connected diodes with four, six, and up to nine diodes, and the equivalent circuits can be seen in the supplementary material. In Fig. 7, these simulation results are shown for (a) all the parameters that we kept the same between the diodes; also, the overall value of the series resistance, which would be globally measured equal, to get a comparable result in terms of the overall shape of the *IV* curve. What can be seen from the second derivative is that with an entirely homogenous device in terms of diode parameters, there is basically no difference between a single diode model and a model with multiple diodes. In (b), we additionally varied the different parameters of the diodes and their associated contact resistance, while a variation of contact resistances within the parameter space we chose does not seem to have an impact. In the variation space we used for the diode ideality factor and the dark saturation current, a multitude of peaks appears. As this did not represent the variation we saw in any of the devices studied, we chose a smaller variation for the dark saturation current, and instead of multiple peaks, we got a

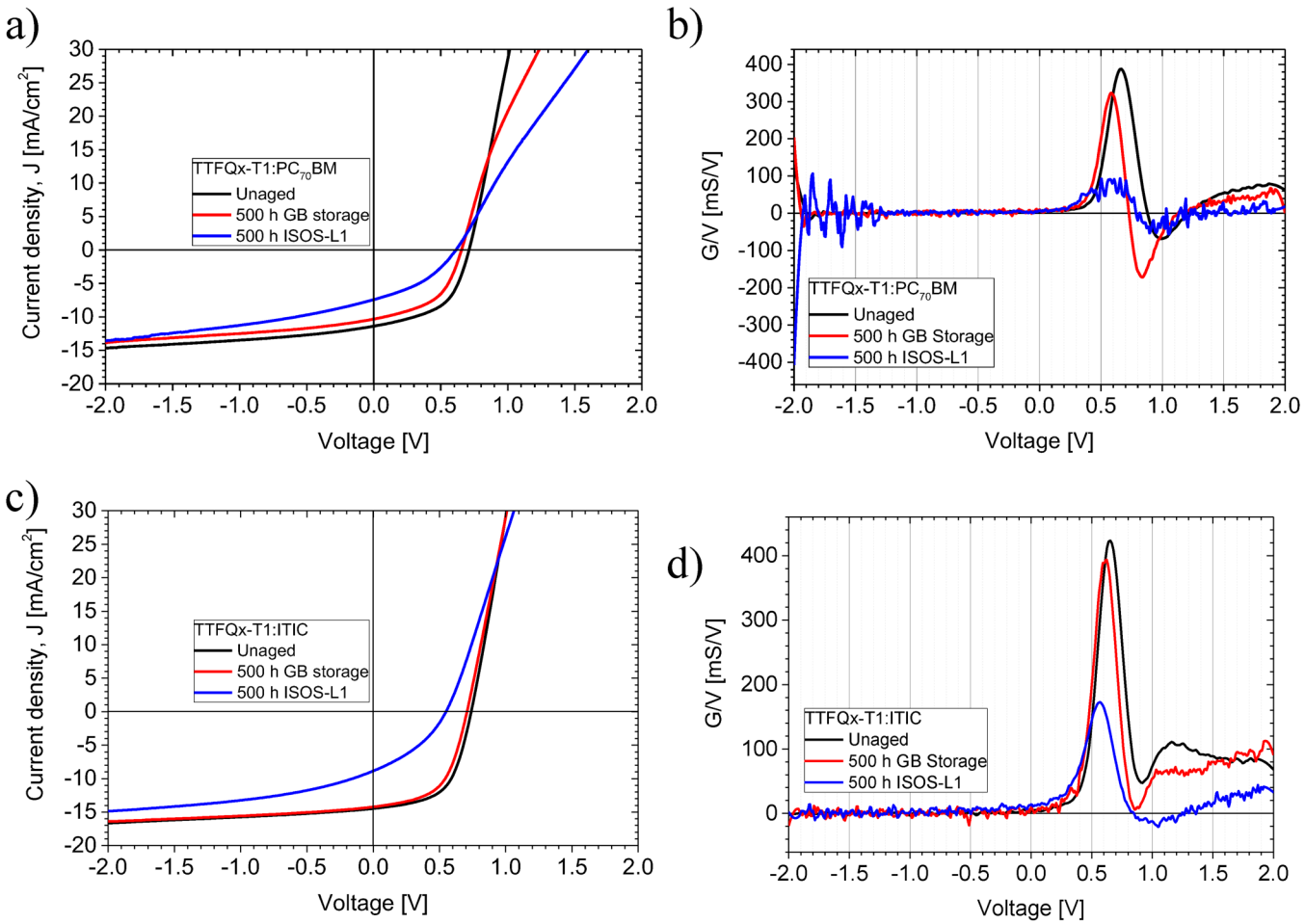

FIG. 10. Conventional organic solar cells with various active layers aged under ISOS-D1 and ISOS-L1 conditions. (a) *IV* curves of unaged and aged TTFQx-T1:$PC_{71}BM$ devices, (b) respective second derivatives to [(a) and (c)] *IV* curves of unaged and aged TTFQx-T1:ITIC devices, (d) respective second derivatives to (c).

peak with a reduced height as well as an increased width. Though this also does not fully quantitatively describe the second derivatives we found for the devices in Fig. 1, we gained a thorough understanding of how different parameters influence the second derivative and how to interpret different shapes.

With the previous simulations and their results, we can now return to the *IV* curves obtained experimentally (compare with Fig. 1). As shown by the simulations, a dual peak is only possible with two parallel diodes, where one of the diodes performs significantly worse than the other. Such a worse performing diode would be especially characterized by a significantly larger dark saturation current. This increase in dark saturation current density could be the result of several factors, like a high doping level, which would lead to a Schottky-like contact at the interface between the organic semiconductor and metal electrode. This likely stems from an inhomogeneous vertical phase separation as one possible effect. The homogenization of performance for devices with a longer soaking time of methanol on top of the active layer film suggests a process driven by diffusion of the material in the active layer as one of the causes for the improvement. However, it cannot be the sole reason; else, the short contact during spin coating would not already show an improvement. Therefore, on the one hand, we propose the formation of a passivating layer due to adsorbed methanol, combined with (at more extended times of methanol exposure) a more favorable vertical phase separation of the blend as the cause for improvement seen from the methanol treatment. We summarized our possible hypothesis why the methanol treatment results in an improvement in Table I, together with an assessment of their probability. Further investigations are ongoing.

Another topic to be mentioned not fully reflected by the simulations done in LTSpice is that all the *IV* curves of well-functioning solar cells do not immediately fall back to zero in the second derivative when the series resistance starts dominating the device behavior. Instead, they tend to stabilize toward a constant value larger

than zero. A short discussion on the possible origin of this effect is given in the supplementary material, as further investigations are ongoing at the moment.

Finally, herein, we also want to show the newly presented method applied to aged organic solar cells. In Fig. 8, the consecutive *IV* curves of devices aged under ISOS-L1[23,24] conditions with a white light LED at 45 °C are shown. The devices consisted of a layerstack of ITO/PEDOT:PSS[PVP AI 4083)/PCDTBT:$PC_{71}BM$/Al. As can be seen in Fig. 8(a), a very subtle S-shape in the *IV* curve toward the end of the 24 h of aging has been developed, while the device shown in Fig. 8(c) does not show an S-shape at the end of the 24 h. The respective second derivatives of the *IV* curves, shown in Figs. 8(b) and 8(d), show some interesting developments; for (b), one can see that there are clearly two inflection points from the second derivative for the devices showing an S-shape, this dual inflection point develops at around 15 h. There is also some difference in the fresh devices for (b) and (d); both show a rather constant second derivative between 1.5 and 2 V. It should be noted that a constant second derivative can, in principle, be associated with a space-charge-limited current (SCLC), whose development over time displays a possible degradation route. In the case of (b), from the beginning, there is already a very weakly "blocking" contact with a valley in the second derivative. This valley further grows in depth up until 15 h, where it crosses the abscissa, and thereupon, keeps further moving toward negative values. A similar trend is shown in (d), but the valley is not there from the start of the experiment and also does not reach negative values. Therefore, the *IV* curve also does not show an S-shape even for the longest times shown here, but from the development of (b), the formation of an S-shape is expected. Another interesting observation is that the peaks in (b) and (d) show broad extensions toward voltages of 0 V. From the simulations shown in Figs. 4 and 7, that very broad extension of this peak can only be explained by a broad distribution of the values of I_0 and/or R_S of the devices. Upon aging, this distribution also shifts toward lower voltages, showing an inhomogeneous degradation of I_0 and/or R_S. In Fig. 9, the development of a blocking contact that takes up more and more of the solar cell area is shown; besides the plateau toward larger biases, it is well able to reproduce the behavior seen in the devices shown in Fig. 8. Note that the equivalent circuits for this simulation are shown in Figs. S57–S61 in the supplementary material. Though it can show the behavior we have seen in the aged devices sufficiently well, we are not ruling out other mechanisms.

In Fig. 10, an additional sample of the aged organic solar cell devices is depicted, which exhibits a conventional layer architecture of glass/ITO/PEDOT:PSS/photoactive layer/Mg/Al. For the fullerene-based device, there is already a weak blocking contact visible in the second derivative for the fresh device, severe enough to result in an S-shape in the *IV* curve. This blocking contact becomes even more severe after 500 h of glovebox storage. As the storage in the glovebox precludes effects like oxidation of the low work function electrodes, the most likely culprit for the observed effect is an unfavorable vertical phase separation of the donor and acceptor, i.e., the polymer is preferentially segregating toward the Mg contact and vice versa. This effect becomes even more severe under ISOS-L1 conditions, as the increased temperature is driving forward the diffusion-driven process more quickly. In the ITIC based device, there is also some blocking character visible in the second derivative, but it is not fully able to block the current in the forward direction. This suggests a reduced driving force for vertical phase separation of the donor and acceptor, in contrast to the combination of the fullerene acceptor. Upon glovebox storage, the blocking contact also got more pronounced without resulting in an S-shape in the *IV* curve. Already during 500 h of ISOS-L1 aging, an S-shape in the *IV* curve has been formed. Besides that, there is a pronounced reduction in peak height in the second derivative without a large shift in position. This suggests a combined increase in diode ideality factor and series resistance with an additional increase in dark saturation current. All mentioned effects would result in a peak reduction, while an increase in diode ideality factor and series resistance would move the peak toward lower voltages, while an increase in diode ideality factor results in the peak moving toward higher voltages compensating for the increase in the other two metrics.

IV. CONCLUSION

Concluding, we have presented a new method to analyze the defects in solar cells via the usage of already existing data from measurements routinely performed as the most basic procedure for any solar cell. This method allows for quick hypothesis generation and can, therefore, assist researchers to focus their efforts on more specific methods. Furthermore, it can be used in aging experiments of the solar cells as an early warning proxy for significant changes in the device to come, as it can detect subtle changes in the *IV* curve with ease. The latter itself is the one measure that is probed throughout the whole experiment—usually during aging experiments—and, therefore, readily available for analysis. Therefore, a steady analysis of the second derivative of *IV* characteristics allows researchers to retrieve samples from an aging experiment at times, where the most important knowledge can be gained on the changes responsible for degradation. We further have presented that the assumption of a simple Shockley equation with series and shunt resistance cannot be enough to adequately describe the behavior of organic solar cells as this is also the basis behind the operation of SPICE and none of the simulated second derivative curves were fully able to represent the measured curves, not even fully qualitatively.

SUPPLEMENTARY MATERIAL

See the supplementary material for additional *IV* curves, all equivalent circuits including the parameters used, and an additional calculation regarding the possible origin of the plateau seen at forward biases above 1 V, in all measured *IV* curves.

ACKNOWLEDGMENTS

R.M., H.H., and U.S.S. gratefully acknowledge the Deutsche Forschungsgemeinschaft (DFG) for financial support. U.S.S. is grateful to the Thüringer Ministerium für Wirtschaft, Wissenschaft und Digitale Geselschaft (TMWWDG) for funding the CEEC Jena. The project underlying these results was funded by the Free State of Thuringia under No. 2016 IZN 0009 and co-financed by funds from the European Union within the framework of the European Regional Development Fund (ERDF). S.A. and F.L. are grateful for

the support from the King Abdullah University of Science and Technology (KAUST) Office of Sponsored Research (OSR) under Award No. OSR-2018-CARF/CCF-3079.

AUTHOR DECLARATIONS

Conflict of Interest

The authors have no conflicts to disclose.

Author Contributions

Rico Meitzner: Conceptualization (equal); Data curation (equal); Formal analysis (equal); Investigation (equal); Methodology (equal); Project administration (equal); Software (equal); Writing – original draft (equal); Writing – review and editing (equal). **Jose Prince Madalaimuthu:** Formal analysis (supporting); Investigation (supporting). **Shahidul Alam:** Data curation (supporting); Formal analysis (supporting); Investigation (supporting). **Md Moidul Islam:** Investigation (supporting). **Sebastian Peiler:** Investigation (supporting). **Aman Anand:** Investigation (supporting); Writing – original draft (supporting). **Johannes Ahner:** Investigation (supporting). **Martin D. Hager:** Funding acquisition (equal); Investigation (supporting). **Ulrich S. Schubert:** Funding acquisition (lead); Writing – original draft (supporting). **Yingping Zou:** Funding acquisition (equal); Investigation (supporting). **Frédéric Laquai:** Funding acquisition (equal); Investigation (equal); Writing – original draft (equal). **Harald Hoppe:** Funding acquisition (equal); Supervision (lead); Writing – original draft (equal).

DATA AVAILABILITY

The data that support the findings of this study are available from the corresponding author on reasonable request.

REFERENCES

[1]N. Espinosa, M. Hosel, M. Jorgensen, and F. C. Krebs, Energy Environ. Sci. **7**(3), 855–866 (2014).
[2]A. Distler, C. J. Brabec, and H.-J. Egelhaaf, Prog. Photovoltaics: Res. Appl. **29**(1), 24–31 (2021).
[3]S. Dong, T. Jia, K. Zhang, J. Jing, and F. Huang, Joule **4**(9), 2004–2016 (2020).
[4]R. Meitzner, U. S. Schubert, and H. Hoppe, Adv. Energy Mater. **11**(1), 2002551 (2021).
[5]C. J. M. Emmott, J. A. Röhr, M. Campoy-Quiles, T. Kirchartz, A. Urbina, N. J. Ekins-Daukes, and J. Nelson, Energy Environ. Sci. **8**(4), 1317–1328 (2015).
[6]Y. Liu, P. Cheng, T. Li, R. Wang, Y. Li, S.-Y. Chang, Y. Zhu, H.-W. Cheng, K.-H. Wei, X. Zhan, B. Sun, and Y. Yang, ACS Nano **13**(2), 1071–1077 (2019).
[7]Q. Liu, Y. Jiang, K. Jin, J. Qin, J. Xu, W. Li, J. Xiong, J. Liu, Z. Xiao, K. Sun, S. Yang, X. Zhang, and L. Ding, Sci. Bull. **65**(4), 272–275 (2020).
[8]N. Espinosa, M. Hosel, D. Angmo, and F. C. Krebs, Energy Environ. Sci. **5**(1), 5117–5132 (2012).
[9]N. Espinosa, Y.-S. Zimmermann, G. A. Dos Reis Benatto, M. Lenz, and F. C. Krebs, Energy Environ. Sci. **9**(5), 1674–1680 (2016).
[10]R. Sun, W. Wang, H. Yu, Z. Chen, X. Xia, H. Shen, J. Guo, M. Shi, Y. Zheng, Y. Wu, W. Yang, T. Wang, Q. Wu, Y. Yang, X. Lu, J. Xia, C. J. Brabec, H. Yan, Y. Li, and J. Min, Joule **5**(6), 1548–1565 (2021).
[11]Y. Li, X. Huang, K. Ding, H. K. M. Sheriff, L. Ye, H. Liu, C.-Z. Li, H. Ade, and S. R. Forrest, Nat. Commun. **12**(1), 5419 (2021).
[12]A. Kumar, S. Sista, and Y. Yang, J. Appl. Phys. **105**(9), 094512 (2009).
[13]G. del Pozo, B. Romero, and B. Arredondo, Sol. Energy Mater. Sol. Cells **104**, 81–86 (2012).
[14]A. Pozza, G. Bardizza, T. Sample, and E. Dunlop, "Analysis based on I-V curve changes of organic photovoltaic mini-modules subjected to degradation under different temperature and humidity conditions," in *29th European Photovoltaic Solar Energy Conference and Exhibition*, Amsterdam, Netherlands, 22-26 September (2014).
[15]L. W. P. D. O. Nagel, *SPICE Simulation Program with Integrated Circuit Emphasis* (Electronics Research Laboratory, College of Engineering, University of California, Berkeley, 1973).
[16]L. Zuo, J. Yao, H. Li, and H. Chen, Sol. Energy Mater. Sol. Cells **122**, 88–93 (2014).
[17]S. Yoo, B. Domercq, and B. Kippelen, J. Appl. Phys. **97**(10), 103706 (2005).
[18]B. Ecker, H.-J. Egelhaaf, R. Steim, J. Parisi, and E. von Hauff, J. Phys. Chem. C **116**(31), 16333–16337 (2012).
[19]J. C. Wang, X. C. Ren, S. Q. Shi, C. W. Leung, and P. K. L. Chan, Org. Electron. **12**(6), 880–885 (2011).
[20]S. R. Cowan, P. Schulz, A. J. Giordano, A. Garcia, B. A. MacLeod, S. R. Marder, A. Kahn, D. S. Ginley, E. L. Ratcliff, and D. C. Olson, Adv. Funct. Mater. **24**(29), 4671–4680 (2014).
[21]S. Trost, T. Becker, A. Polywka, P. Görrn, M. F. Oszajca, N. A. Luechinger, D. Rogalla, M. Weidner, P. Reckers, T. Mayer, and T. Riedl, Adv. Energy Mater. **6**(15), 1600347 (2016).
[22]R. Meitzner, J. Essomba, S. Alam, A. Anand, N. Engel, K. Fulbert, K. Kuma, F. Ayuyasmin, M. M. Islam, C. Ugokwe, U. S. Schubert, and H. Hoppe, Energy Technol. **8**(12), 2000117 (2020).
[23]M. O. Reese, S. A. Gevorgyan, M. Jørgensen, E. Bundgaard, S. R. Kurtz, D. S. Ginley, D. C. Olson, M. T. Lloyd, P. Morvillo, E. A. Katz, A. Elschner, O. Haillant, T. R. Currier, V. Shrotriya, M. Hermenau, M. Riede, K. R. Kirov, G. Trimmel, T. Rath, O. Inganäs, F. Zhang, M. Andersson, K. Tvingstedt, M. Lira-Cantu, D. Laird, C. McGuiness, S. Gowrisanker, M. Pannone, M. Xiao, J. Hauch, R. Steim, D. M. DeLongchamp, R. Rösch, H. Hoppe, N. Espinosa, A. Urbina, G. Yaman-Uzunoglu, J.-B. Bonekamp, A. J. J. M. van Breemen, C. Girotto, E. Voroshazi, and F. C. Krebs, Sol. Energy Mater. Sol. Cells **95**(5), 1253–1267 (2011).
[24]M. V. Khenkin, E. A. Katz, A. Abate, G. Bardizza, J. J. Berry, C. Brabec, F. Brunetti, V. Bulović, Q. Burlingame, A. Di Carlo, R. Cheacharoen, Y.-B. Cheng, A. Colsmann, S. Cros, K. Domanski, M. Dusza, C. J. Fell, S. R. Forrest, Y. Galagan, D. Di Girolamo, M. Grätzel, A. Hagfeldt, E. von Hauff, H. Hoppe, J. Kettle, H. Köbler, M. S. Leite, S. Liu, Y.-L. Loo, J. M. Luther, C.-Q. Ma, M. Madsen, M. Manceau, M. Matheron, M. McGehee, R. Meitzner, M. K. Nazeeruddin, A. F. Nogueira, Ç Odabaşı, A. Osherov, N.-G. Park, M. O. Reese, F. De Rossi, M. Saliba, U. S. Schubert, H. J. Snaith, S. D. Stranks, W. Tress, P. A. Troshin, V. Turkovic, S. Veenstra, I. Visoly-Fisher, A. Walsh, T. Watson, H. Xie, R. Yıldırım, S. M. Zakeeruddin, K. Zhu, and M. Lira-Cantu, Nat. Energy **5** (1), 35–49 (2020).
[25]See https://www.analog.com/en/design-center/design-tools-and-calculators/ltspice-simulator.html for information regarding LTSpice: Analog Devices (Last viewed 16 May 2022)